

Cross Correlating 21 cm Signal with Kinematic Sunyaev-Zel'dovich Effect: A New Probe for Missing Baryons at $z \sim 1 - 2$

Dongzi Li,^{1,2} Ue-Li Pen,^{3,4,5,1} Hong-Ming Zhu,^{6,7} and Yu Yu⁸

¹*Perimeter Institute for Theoretical Physics, 31 Caroline St. N., Waterloo, ON, N2L 2Y5, Canada*

²*University of Waterloo, 200 University Ave W, Waterloo, ON, N2L 3G1, Canada*

³*Canadian Institute for Theoretical Astrophysics, 60 St. George Street, Toronto, Ontario M5S 3H8, Canada*

⁴*Dunlap Institute for Astronomy and Astrophysics, 50 St. George Street, Toronto, Ontario M5S 3H4, Canada*

⁵*Canadian Institute for Advanced Research, CIFAR Program in Gravitation and Cosmology, Toronto, Ontario M5G 1Z8, Canada*

⁶*Key Laboratory for Computational Astrophysics, National Astronomical Observatories, Chinese Academy of Sciences, 20A Datun Road, Beijing 100012, China*

⁷*University of Chinese Academy of Sciences, Beijing 100049, China*

⁸*Key laboratory for research in galaxies and cosmology, Shanghai Astronomical Observatory, Chinese Academy of Sciences, 80 Nandan Road, Shanghai 200030, China*

(Dated: May 27, 2016)

The kinematic Sunyaev-Zel'dovich (kSZ) effect on cosmic microwave background (CMB), induced by radial momentum of hot electrons, is a powerful tracer to probe baryon distributions. However, the signal is weak and lack of redshift information, hence another survey with spectroscopic redshift is typically required. This largely limits the sky area and depth to harness kSZ. Here, we propose a new source for cross correlation—H I density field from 21 cm intensity mapping. 21 cm spectra provide accurate redshift and intensity mappings integrate weak diffuse spectra, and thus can survey large sky area with great depth in much shorter time with low costs.

One main concern of the method is that the complicate 21 cm foregrounds will contaminate radial large scale information, and reduce the correlation with kSZ. For redshift 1 and 2, we model the noise filtering in simulations, and find out that after velocity reconstructions, there is $\gtrsim 0.7$ correlation with kSZ signal for $\ell \gtrsim 800$, and it drops for smaller ℓ . To improve the correlation for smaller ℓ , we recover large scale modes from their tidal influence on small scale structures (Cosmic Tidal Reconstruction). Successfully recover $> 90\%$ information at $k \sim 0.01 h/Mpc$, we obtain a correlation $r \sim 0.6 - 0.8$ for $\ell \sim 100 - 2000$. The overall S/N for $\ell \sim 300 - 4000$ assuming Planck noise scale can reach 45 at $z = 1$, and 59 at $z = 2$. Since the reconstructed field and foreground filtered field are superior in different modes, it is easy to combine them and improve S/N for $\ell \sim 1000$.

PACS numbers:

I. INTRODUCTION

While the baryon abundance of early universe is well fixed [1–4], for $z \lesssim 2$, large fractions of baryons are missing in observations. The majority of them are believed to reside in Warm-Hot Intergalactic Mediums (WHIM) with typical temperature of 10^5 K to 10^7 K [5, 6], which is too hot and diffuse to detect. Progress has been made in recent years to detect colder fraction of WHIM using absorption lines (e.g. H I, broad Ly α , Mg II, Si II, C II, Si III, C III, Si IV, O VI, O VII) [7, 8], yet not much detection can reach $T \gtrsim 10^6$ K. Besides, these detections are usually biased towards collapsed objects, and metal lines have to suffer from the great uncertainty on ionization states and metallicity.

A more promising tracer for missing baryons is the kinematic Sunyaev-Zel'dovich (kSZ) effect [9–11], which results from Compton scattering of cosmic microwave background (CMB) off free electrons. The radial velocity of electrons will give photon a Doppler shift and hence leads to a secondary anisotropy in CMB temperature. The kSZ signal has lots of advantages: First, it is contributed from the absolute majority of baryons, leaving alone only less than 10% of baryons that reside in stars, remnants, atomic and molecular gases [12]. The fraction is rather stable. Second, it only relates to electron density and radial velocity, regardless the temperature, pressure or metallicity, so no extra assumptions are needed to estimate baryon abundance. Third, velocity mainly results from large

scale structure, therefore the method is less biased towards local mass contraction.

Attractive as it is, due to the contamination from primary CMB, facility noises, thermal SZ effect and CMB lensing, it is difficult to filter for the kSZ signal independently. Worse still, the signal itself does not contain redshift information. Therefore, previous approaches tend to cross correlate it with galaxy spectroscopic surveys, which has large scale information and accurate redshift. Yet, it is difficult and costly for this kind of survey to cover large sky area and probe high redshift. A recent effort attempts to relax the condition using projected fields of galaxies from photometric surveys, which are highly accessible [13, 14]. However, projected fields only maintain the largest scale information in z direction, while for $\ell \gtrsim 1000$, where primary CMB fades away, a sufficient amount of kSZ signal comes from intermediate scales. This limits the overall S/N it can reach.

In this paper we put forward a new tracer for cross correlation—H I density field from 21 cm intensity mapping. H I 21 cm spectra have accurate redshift information. And intensity mapping, since it integrates signals rather than distinguishing individual galaxies, can accumulate contributions from weak sources and reach high S/N much faster. There are already several ongoing experiments aim at large sky coverage and claim to be able to reach $z \gtrsim 1$ in very near future, such as CHIME [15], Tianlai [16], HIRAX [17] etc. Therefore, this correlator is more feasible than large galaxy spectroscopic

surveys, and more accurate that projected field.

However, the 21 cm density field has its own drawback—the complicated foregrounds result from integration. While a cosmic signal in 21 cm measurement is of the order of mK, foregrounds coming from Galactic emissions, telescope noise, extragalactic radio sources and Radio recombination lines, can reach the order of Kelvin [18, 19]. Lots of techniques have been developed to filter the foregrounds, taking advantage of the attribute that they have fewer bright spectral degrees of freedom [20]. Unfortunately, the manipulation will contaminate the smooth large scale structure in radial direction, and hence degrade the correlation with kSZ signal.

In this paper, we first evaluate the influence of foregrounds and other noises on the cross correlation. We then apply a method, cosmic tidal reconstruction [21, 22], to recover the large scale structure from its tidal influence on small scales and see the improvement on correlation coefficients.

The paper is organized as follows: In section II, we demonstrate given a density field, how to correlate it with kSZ signal with velocity reconstruction, similar to [23]; In section III, we present the result of cross correlation with foreground filtered field and discuss the behavior; Then in section IV, we introduce the method of 3D tidal reconstruction, and present the correlation results after small k modes recovered, In section V, we discuss redshift space distortions; In section VI, we estimate statistical error and calculate S/N; and we conclude at section VII.

Notes: Throughout the paper, We use the $z = 1, 2$ output of six N -body simulations from the CUBEP³M code [24], each evolving 1024^3 particles in a $(1.2\text{Gpc}/h)^3$ box. Simulation parameters are as follows: Hubble parameter $h = 0.678$, baryon density $\Omega_b = 0.049$, dark matter density $\Omega_c = 0.259$, amplitude of primordial curvature power spectrum $A_s = 2.139 \times 10^{-9}$ at $k_0 = 0.05 \text{ Mpc}^{-1}$ and scalar spectral index $n_s = 0.968$.

we use “ \wedge ” to denote reconstructed fields as oppose to fields directly from simulations.

II. KSZ RECONSTRUCTION

The CMB temperature fluctuations caused by kSZ effect is:

$$\Theta_{kSZ}(\hat{n}) \equiv \frac{\Delta T_{kSZ}}{T_{\text{CMB}}} = -\frac{1}{c} \int d\eta g(\eta) \mathbf{p}_{\parallel}, \quad (1)$$

where $\eta(z)$ is the comoving distance at redshift z , $g(\eta) = e^{-\tau} d\tau/d\eta$ is the visibility function, τ is the optical depth to Thomson scattering, $\mathbf{p}_{\parallel} = (1 + \delta)\mathbf{v}_{\parallel}$, with δ the electron overdensity, \parallel indicates direction parallel to line of sight. We assume that $g(\eta)$ doesn't change significantly in one redshift bin, and integrate \mathbf{p}_{\parallel} along radial axis to get $\hat{\Theta}_{kSZ}$.

Due to the cancellation of positive and negative velocity, its direct cross correlation between kSZ signal will vanish. To better maintain the one to one multiplication between velocity field and density contrast, we first calculate the linear peculiar velocity, and then generate a mock kSZ signal [23]. In this way, we can at most maximize the correlation.

Assume we have a density contrast field $\delta = (\rho - \bar{\rho})/\bar{\rho}$, where $\bar{\rho}$ is the average density of a certain redshift slice.

Detailed steps are as follows.

(1) Estimate the velocity field:

In linear region, the continuity equation goes like: $\dot{\delta} + \nabla \cdot \mathbf{v} = 0$, where \mathbf{v} is the peculiar velocity and δ is the matter overdensity.

Therefore, we obtain an estimator of velocity distribution from the density contrast δ :

$$\hat{v}_z(\mathbf{k}) = iaHf\delta(\mathbf{k}) \frac{k_z}{k^2} \quad (2)$$

where $f = d\ln D/d\ln a$, $D(a)$ is the linear growth function, a is the scale factor, H is the Hubble parameter.

$v_z \propto k_z/k^2$, indicating the most prominent signal comes from small k mode, which corresponds to large scale structure.

(2) suppress the noise in velocity field with a Wiener filter. This is because the term k_z/k^2 in Eq.(2) will strongly amplify noises in small k modes.

$$\hat{v}_z^c(\mathbf{k}) = \frac{\hat{v}_z(\mathbf{k})}{b(k_{\perp}, k_{\parallel})} W(k_{\perp}, k_{\parallel}), \quad (3)$$

Bias $b = P_{\hat{v}_z, v_z}/P_{v_z}$, Wiener filter $W = P_{v_z}/(P_{\hat{v}_z}/b^2)$.

(3) Calculate 2D kSZ map follow Eq.(1).

(4) Calculate correlation coefficients.

We compare reconstructed kSZ signals $\hat{\Theta}_{kSZ}$ with kSZ signals Θ_{kSZ} directly from simulations. To quantify the tightness of correlation, we employ a quantity r :

$$r \equiv \frac{P_{\text{recon}, \text{real}}}{\sqrt{P_{\text{recon}} P_{\text{real}}}} \quad (4)$$

III. CROSS CORRELATION WITH NOISE SUBTRACTED 21 CM FIELD

A. Mimic Noise Subtraction

To resemble realistic observations, we take into account the resolution, small scale noises and foreground subtractions. Two filters are applied on original density contrast δ to imitate the effects of noise subtractions:

1. For small scale noises:

Import a cut off scale k_c with a step function $H(k_c - k)$. For $k > k_c$, $H(k_c - k) = 0$; for $k \leq k_c$, $H(k_c - k) = 1$. This is reasonable for a single dish experiment, which has good brightness sensitivity and an exponentially growing noise at small scales. We choose $k_c = 0.5 h/\text{Mpc}$ and $0.32 h/\text{Mpc}$ respectively for $z = 1$ and $z = 2$, which corresponds to $\ell \sim 1150$. This is generally realistic, judging from ongoing 21 cm experiments like CHIME [15][25] and Tianlai [26][16].

2. For foreground noises:

Use a high pass filter $W_{fs}(k_{\parallel}) = 1 - e^{-k_{\parallel}^2 R_{\parallel}^2/2}$ to imitate the subtraction. We choose $R_{\parallel} = 15 \text{ Mpc}/h$ for $z = 1$ and $R_{\parallel} = 8 \text{ Mpc}/h$ for $z = 2$, which gives $W_{fs} = 0.5$ at $k_{\parallel} = 0.08 \text{ Mpc}/h$ and $0.15 \text{ Mpc}/h$ respectively.

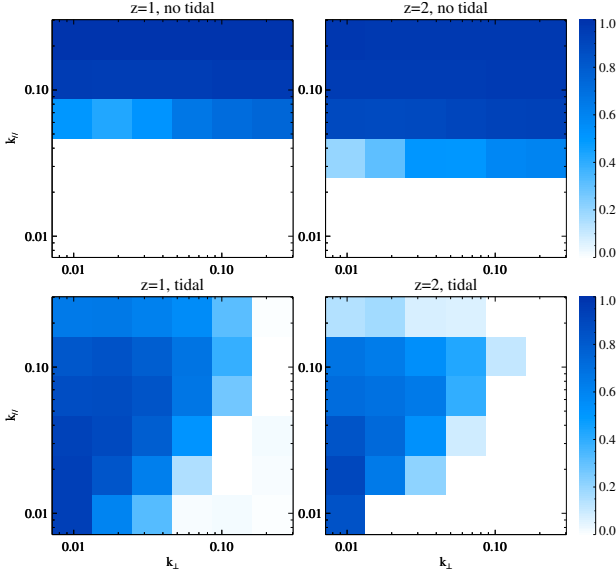


FIG. 1: (Top) The cross correlation r between P_{v_z} and $P_{\hat{v}_{fs}}$ calculated from foreground filtered field δ_{fs} ; (Bottom) The cross correlation between P_{v_z} and $P_{\hat{v}_{z}^{tide}}$ calculated from $\hat{\kappa}_c$.

The observed 21 cm field after noises subtraction is then given by

$$\delta_{ns}(\mathbf{k}) = \delta(\mathbf{k})W_{fs}(k_{\parallel})H(k_c - k), \quad (5)$$

With the noise filtered density contrast δ_{ns} , we follow the procedure described in section II to generate a mock kSZ signal $\hat{\Theta}_{ns}$ and calculate cross correlation $r_{\Theta\hat{\Theta}_{ns}}$.

B. Cross Correlation with Noise Subtracted Field

Fig.1 upper panel Shows the cross correlation between the reconstructed velocity field $\hat{v}_{z,ns}$ and the real velocity field v_z , at redshift 1 and 2.

At this point, all the manipulation and calculation on $\delta(\mathbf{k})$ are independent over different \mathbf{k} , therefore, the cross-correlation closely resembles the subtraction we perform. Just one interesting thing to notice is that although the foreground at $z = 2$ is stronger, the non-linear effects are weaker. So we still can obtain correlations at $k_{\parallel} \lesssim 0.1$ with the seriously suppressed density contrast.

Fig.2 black dashed lines show the cross correlation between the reconstructed kSZ map $\hat{\Theta}_{ns}$ and real kSZ map Θ at redshift 1 and 2. There are two points to notice:

(1) For both redshift, there are a considerable amount of correlation $r \gtrsim 0.5$ for $\ell \gtrsim 1000$; and this correlation drops quickly for smaller ℓ ;

(2) The obtained correlation at redshift 2 is better than redshift 1.

Although not satisfactory at small ℓ , the reconstructed kSZ signal $\hat{\Theta}_{ns}$ from 21 cm density field shall already be able to give us reasonable S/N in real applications, because most kSZ signals that can actually be distinguished come from at least $\ell \gtrsim 500$, when primary CMB gradually dies out.

C. Explanation of Correlation Coefficient Fluctuations

To explain the behavior of the cross correlation, we write Eq.(1) in Fourier space.

$$\begin{aligned} \Theta(\mathbf{k}_{\perp}) &\equiv \Theta(k_x, k_y, 0) \propto \int d^3k' \delta(\mathbf{k}_{\perp} - \mathbf{k}'_{\perp}, k'_{\parallel}) v_z(\mathbf{k}') \\ &\xrightarrow[\text{region}]{\text{linear}} \int d^3k' \delta(\mathbf{k}_{\perp} - \mathbf{k}'_{\perp}, k'_{\parallel}) \delta(\mathbf{k}') \frac{k'_z}{k'^2} \end{aligned} \quad (6)$$

$$\begin{aligned} \langle \Theta(\mathbf{k}_{\perp}) \Theta^*(\mathbf{k}_{\perp}) \rangle &\propto \int \frac{d^3\mathbf{k}'}{(2\pi)^3} \frac{d^3\mathbf{k}''}{(2\pi)^3} \frac{k'_z}{k'^2} \frac{k''_z}{k''^2} \\ &\quad \langle \delta(\mathbf{k}') \delta(\mathbf{k}_{\perp} - \mathbf{k}') \delta^*(\mathbf{k}'') \delta^*(\mathbf{k}_{\perp} - \mathbf{k}'') \rangle \end{aligned} \quad (7)$$

The dominate term is $\langle \delta(\mathbf{k}') \delta^*(\mathbf{k}'') \rangle \langle \delta(\mathbf{k}_{\perp} - \mathbf{k}') \delta^*(\mathbf{k}_{\perp} - \mathbf{k}'') \rangle$ and $\langle \delta(\mathbf{k}') \delta^*(\mathbf{k}_{\perp} - \mathbf{k}'') \rangle \langle \delta(\mathbf{k}_{\perp} - \mathbf{k}') \delta^*(\mathbf{k}'') \rangle$, hence,

$$\begin{aligned} \langle \Theta(\mathbf{k}_{\perp}) \Theta^*(\mathbf{k}_{\perp}) \rangle &\propto \int d^3\mathbf{k}' d^3\mathbf{k}'' \frac{k'_z}{k'^2} \frac{k''_z}{k''^2} \\ &\quad P(k') P(\mathbf{k}_{\perp} - \mathbf{k}') [\delta^D(\mathbf{k}' - \mathbf{k}'') + \delta^D(\mathbf{k}' + \mathbf{k}'' - \mathbf{k}_{\perp})] \\ &= \int d^3 \ln \mathbf{k}' \frac{k'_z k'_x k'_y}{k'^2} P(k') P(\mathbf{k}_{\perp} - \mathbf{k}') \left(\frac{1}{k'^2} - \frac{1}{|\mathbf{k}_{\perp} - \mathbf{k}'|^2} \right) \end{aligned} \quad (8)$$

We transform $dk \rightarrow d \ln k$ to show the contributions from different k scales.

For small $k_{\perp} \sim 0.01$ h/Mpc, which corresponds to $\ell \sim 20 - 30$:

Most $(\frac{1}{k'^2} - \frac{1}{|\mathbf{k}_{\perp} - \mathbf{k}'|^2}) \sim \frac{1}{k'^3}$, so we have $k'_z k'_x k'_y / k'^5$ which is scale invariant, and $P(k') P(\mathbf{k}_{\perp} - \mathbf{k}')$ reach peak at similar point with small k . Therefore, main contribution of the powerspectrum is from large scale. On the other hand, the fields after foreground subtraction lack the part from small k , which causes the null correlation.

For large $k_{\perp} \sim 1$ h/Mpc:

$(\frac{1}{k'^2} - \frac{1}{|\mathbf{k}_{\perp} - \mathbf{k}'|^2}) \sim \frac{1}{k'^2}$ or even $\sim \frac{1}{k_{\perp}^2}$ so we have at least $k'_z k'_x k'_y / k'^4$, which prefers small scales. Moreover, $P(k') P(\mathbf{k}_{\perp} - \mathbf{k}')$ no longer reach peak at similar point. Therefore, the importance of small k modes is attenuated, and the influence of foregrounds are reduced.

The reason why the correlation on redshift 2 is better is that the density contrast at redshift 1 is sharper than redshift 2, which exaggerates the contribution from small scales.

IV. CROSS CORRELATION AFTER COSMIC TIDAL RECONSTRUCTION

With noise subtracted 21 cm density field, we are able to have detectable cross correlations for $\ell \gtrsim 800$. However, we are also interested in large scale baryon distributions, which is free from the complicated activities happen in smaller scales. We use Cosmic Tidal Reconstruction to recover correlations for small ℓ and improve correlations for intermediate ℓ . This is one of the first application of its 3D version.

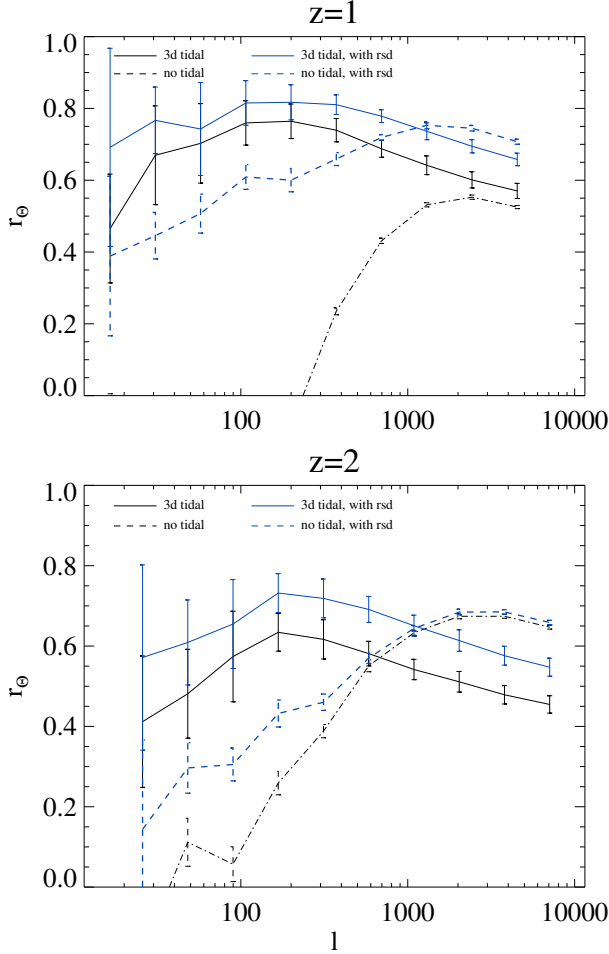


FIG. 2: The cross correlation r between reconstructed kSZ $P_{\Theta_{kSZ}}$ and real kSZ $P_{\Theta_{kSZ}}$. (Dashed line) kSZ calculated from foreground filtered 21 cm density field δ_{fs} ; (Solid line) kSZ calculated from tidal reconstructed density field. (Blue lines) take into account of redshift space distortions.

A. 3D Cosmic Tidal Reconstruction

The fundamental idea of Cosmic Tidal Reconstruction is that the evolution of small scale structure is modulated by large scale gravitational force. We can select this effect and solve for the large scale potential.

Main Procedure:

Consider only the anisotropic influence from tidal force, the distortions on power spectrum [22] can linearly be calculated as

$$\delta P(\mathbf{k}, \tau)|_{t_{ij}} = \hat{k}^i \hat{k}^j t_{ij}^{(0)} P_{1s}(k, \tau) f(k, \tau) \quad (9)$$

where f is the linear coupling function; $P_{1s}(k, \tau)$ is the theoretical small scale linear powerspectrum; and $\delta P(\mathbf{k}, \tau)$ is the real distortion from observations.

Hence we can solve for the unknown quantity t_{ij} , which is the tidal force tensor defined as

$$t_{ij} = \Phi_{L,ij} - \nabla^2 \Phi_L \delta_{ij}^D / 3 \quad (10)$$

$\Phi_{L,ij}$ is the second derivative of large scale potential, δ^D is the Dirac function.

With t_{ij} , we calculate the variance of large scale potential Φ_L and get the large scale density contrast κ_{3D} .

$$\kappa_{3D} \sim \nabla^2 \Phi_L = \frac{3}{2} \nabla^{-2} \partial_i \partial_j t_{ij} \quad (11)$$

Since $f(k, \tau)$ increase with k in our interested scales, the distortions are more obvious in small scales. Therefore, the method mainly use the quadratic statistics on small scales to recover the large scale density field. It works best for close linear regions.

Detailed steps:

(1) Gaussianize the field, taking $\delta_g = \ln(1 + \delta)$. This is to alleviate the problem that filter W_i in Eq.(14) heavily weights high density regions.

(2) Following gravitational lensing procedures, decompose the symmetric, traceless tidal force tensor into 5 components,

$$t_{ij} = \begin{pmatrix} \gamma_1 - \gamma_z & \gamma_{\times} & \gamma_2 \\ \gamma_{\times} & -\gamma_1 - \gamma_z & \gamma_y \\ \gamma_2 & \gamma_y & 2\gamma_z \end{pmatrix}. \quad (12)$$

(3) Select density distortions caused by tidal force, by convolving δ_g with a filter W_i deduced from Eq.(9)

$$\delta_g^{w_i}(\mathbf{k}) = W_i(\mathbf{k}) \delta_g(\mathbf{k}) \quad (13)$$

$$W_i(\mathbf{k}) = i \left[\frac{P(k) f(k)}{P_{tot}^2(k)} \right]^{\frac{1}{2}} \frac{k_i}{k} = S(k) \frac{k_i}{k}$$

where i indicates $\hat{x}, \hat{y}, \hat{z}$ directions, $f(k) = 2\alpha(\tau) - \beta(\tau) d \ln P / d \ln k$ is again the coupling function, with α and β related to linear growth function [22], and calculated to be (0.6, 1.3) for $z = 1$ and (0.4, 0.9) for $z = 2$. $P_{tot} = P + P_{noise}$ is observed matter powerspectrum, P is theoretical matter powerspectrum,

(4) Estimate the 5 tidal tensor components from quadratic statistics.

$$\begin{aligned} \hat{\gamma}_1(\mathbf{x}) &= [\delta_g^{w_1}(\mathbf{x}) \delta_g^{w_1}(\mathbf{x}) - \delta_g^{w_2}(\mathbf{x}) \delta_g^{w_2}(\mathbf{x})], \\ \hat{\gamma}_2(\mathbf{x}) &= [2\delta_g^{w_1}(\mathbf{x}) \delta_g^{w_2}(\mathbf{x})], \\ \hat{\gamma}_x(\mathbf{x}) &= [2\delta_g^{w_1}(\mathbf{x}) \delta_g^{w_3}(\mathbf{x})], \\ \hat{\gamma}_y(\mathbf{x}) &= [2\delta_g^{w_2}(\mathbf{x}) \delta_g^{w_3}(\mathbf{x})], \\ \hat{\gamma}_z(\mathbf{x}) &= \frac{1}{3} [(2\delta_g^{w_3}(\mathbf{x}) \delta_g^{w_3}(\mathbf{x}) \\ &\quad - \delta_g^{w_1}(\mathbf{x}) \delta_g^{w_1}(\mathbf{x}) - \delta_g^{w_2}(\mathbf{x}) \delta_g^{w_2}(\mathbf{x}))], \end{aligned} \quad (14)$$

(5) Reconstruct large scale density contrast κ_{3D} from tidal tensor:

$$\begin{aligned} \kappa_{3D}(\mathbf{k}) &= \frac{1}{k^2} [(k_1^2 - k_2^2) \gamma_1(\mathbf{k}) + 2k_1 k_2 \gamma_2(\mathbf{k}) \\ &\quad + 2k_1 k_3 \gamma_x(\mathbf{k}) + 2k_2 k_3 \gamma_y(\mathbf{k}) \\ &\quad + (2k_3^2 - k_1^2 - k_2^2) \gamma_z(\mathbf{k})]. \end{aligned} \quad (15)$$

(6) Correct bias and suppress noise with a Wiener filter.

Due to the foregrounds, the noise in z direction will be different from x, y direction, therefore we apply an anisotropic Wiener filter.

$$\hat{\kappa}_c(\mathbf{k}) = \frac{\kappa_{3D}(\mathbf{k})}{b(k_\perp, k_\parallel)} W(k_\perp, k_\parallel), \quad (16)$$

Bias $b(k_\perp, k_\parallel) = P_{\kappa_{3D}, \delta} / P_\delta$ is the cross powerspectra between reconstructed field κ_{3D} and original field δ , Wiener filter $W(k_\perp, k_\parallel) = P_\delta / (P_{\kappa_{3D}} / b^2)$.

Here $\hat{\kappa}_c$ is the output large scale density contrast we obtain from tidal reconstruction. We use it to calculate velocity \hat{v}_z^{tide} and mock kSZ signal $\hat{\Theta}_{\text{tide}}$ following identical procedure as to noise filtered field.

B. Cross Correlation with Tidal Reconstructed Field

For comparison, we first present the cross correlation between v_z and \hat{v}_z^{tide} in lower panels of Fig.1.

It is obvious that the previously lost small k_\parallel modes are partly recovered. The reconstruction on k_\parallel direction is better than on k_\perp direction. This is because tidal reconstruction relies heavily on large k modes, yet lots of large k_\perp modes, whose k_\parallel is small, are lost in the foregrounds. There is degrading performance of tidal reconstruction on $z = 2$ compared to $z = 1$, which mainly results from the stricter cutoff $k_c = 0.32$ h/Mpc compared to $k_c = 0.5$ h/Mpc.

In Fig.2, we demonstrate the correlation r between the reconstructed kSZ signal $\hat{\Theta}_{\text{tide}}$ and original kSZ signal Θ .

It is important to see: For $z = 1$, there are significant improvement on the cross-correlation after tidal reconstruction, especially below $\ell \sim 2000$; for $z = 2$, the cross-correlation is improved for $\ell \lesssim 800$. Combining noise filtered fields and tidal reconstructed fields, we shall have good cross-correlation for $\ell \sim 50 - 5000$, with the assumed level of foregrounds and noises on small scales.

C. Possible Improvements on Tidal Reconstruction

In section IV B we present the result of the simplest tidal reconstruction. However, since our noises are strongly dependent on direction and scale, there are several steps that can help obtain more accurate reconstruction.

First, there is a $P_{\text{tot}} = P + P_{\text{noise}}$ in the denominator of the filter W_i in Eq.14. Previously, we simply set $P_{\text{tot}} = P$. A more accurate way to select relevant distortions is to consider different noise level of different scales. We can estimate the noise spectra in simulation with $P_{\text{noise}}(k_\perp, k_\parallel) = P_{\delta, n.s.}(k_\perp, k_\parallel) - b^2(k_\perp, k_\parallel) P_\delta(k_\perp, k_\parallel)$, where b is again the bias. After that, we apply different renormalization to γ in eq.14. The effect is to assign heavier weights to large z , where signals are cleaner.

Second, since different γ use different modes, their noise and bias are different. It is better to filter them separately before combining together. Follow Eq.11, we could estimate the expected value of γ with $t_{ij} \sim \frac{2}{3} \frac{k^2}{k_i k_j} \delta$, where δ is the original

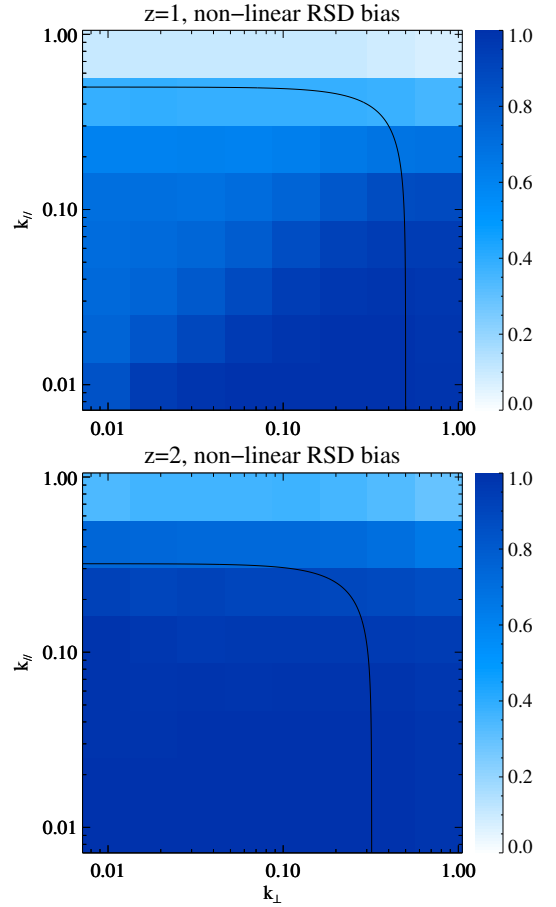


FIG. 3: The bias $b = P_{\delta_{\text{nlRSD}}, \delta} / P_\delta$ of redshift space distorted(RSD) field after linear RSD subtraction. Dark lines indicate the k_c cutoff—modes above them are assumed to be lost in noise.

field with complete large scale structure. After that, we apply Wiener filter similar to Eq.16 to each γ before calculating κ_{3D} . This measurement will better suppress the noises and assign heavier weights to shear estimators related to z direction. This is again because of the more intact information of small scale structure in z direction.

V. REDSHIFT SPACE DISTORTIONS

The redshift space distortion(RSD) refers to the misjudgment on comoving distance resulting from peculiar velocity of objects. In this section we add the RSD effect to our original fields and present the cross correlation result in Fig.2. The influence is quite interesting.

First, there is an improvement on tidal reconstruction results, which increases the cross correlation by 0.1 for nearly all ℓ demonstrated. Second, for noise subtracted fields, the correlation on intermediate scales start to emerge.

All these unexpected improvements can be attributed to the fortunate fact that RSD is in identical direction with foregrounds. The different behaviors are due to linear and non-linear RSD.

Linearly RSD will induce an additional contraction in z direction which increases with z . $\delta^{\text{RSD}}(\mathbf{k}) = (1 + f\mu^2)\delta(\mathbf{k})$ with $\mu = k_{\parallel}/k$. If we divide the observed density contrast with $1 + f\mu^2$, we can see how much non-linear effect presents. we show the bias between linearly subtracted RSD field and real space field in Fig.3. Dark lines indicate the small scale cut off. As we can see, for $z = 2$, the modes we use are generally within linear RSD regions; for $z = 1$, linear RSD still dominates, yet there are considerable non-linear RSD for large k_{\parallel} .

The positive effect on tidal reconstruction is mainly caused by linear RSD—that's why it is stronger on $z = 2$ than $z = 1$. The additional contraction $1 + f\mu^2$ assigns more weights to larger k_z modes, and give a preference on $\gamma_x, \gamma_y, \gamma_z$ in Eq.14. This happen to be consistent with the improvements we suggest in Section IV C, which reduces the weights of foreground contaminated modes, and increases the dependence on three shear estimators that are relatively clean. Therefore, the recovering results will better assemble original fields.

For noise subtracted fields, the higher cross correlations on large scales are caused by non-linear RSD. The contraction from linear RSD is corrected in Eq.3 by dividing the bias term. However, the non-linear RSD will induce extra noises that can not be directly suppressed by bias, and will lead to reduced weights in Wiener filter for small scale structure. Consider previously the null correlation is due to reduced weights on large scales due to foreground contamination. Now the small scale distortions somewhat rebalance the weights, which results to the appearance of a little correlation on smaller ℓ . This effect is mainly seen on $z = 1$ with stronger non-linear RSD.

In all, the RSD seems to be a blessing rather than a problem in our case. It also reveals the great potential of our reconstruction if applying more precise noise-related filter. And this is not the only advantage RSD brings. In reality, the inhancement in large k_z will increase the S/N, and therefore raise the cut off scale k_c , which enables better tidal reconstruction results.

VI. STATISTICAL ERROR

We use the statistical error to estimate the S/N ratio for real surveys, taking into account the contamination from primary CMB and facility noises.

$$\frac{S}{N} = \frac{C_l}{\Delta C_l} \quad (17)$$

$$\simeq r \sqrt{(2\ell + 1) \Delta l f_{\text{sky}}} \sqrt{\frac{C_l^{\text{kSZ}, \Delta z}}{C_l^{\text{CMB}} + C_l^{\text{kSZ}} + C_l^{\text{CMB}, N}}}$$

Where C_l^{CMB} is the angular powerspectrum of primary CMB; $C_l^{\text{CMB}, N}$ indicates the facility noises; $C_l^{\text{kSZ}, \Delta z}$ is the kSZ signal from a certain redshift bin; r is the correlation coefficients we get; f_{sky} is the percent of sky area covered by both surveys.

In our case, we calculate C_l^{CMB} from CAMB [27]. We use Planck 2015 results [28] at 217GHz to estimate $C_l^{\text{CMB}, N}$. $C_l^{\text{CMB}, N} = (\sigma_{p,T} \theta_{\text{FWHM}})^2 W_l^{-2}$; where $\sigma_{p,T} = 8.7 \mu K_{\text{CMB}}$

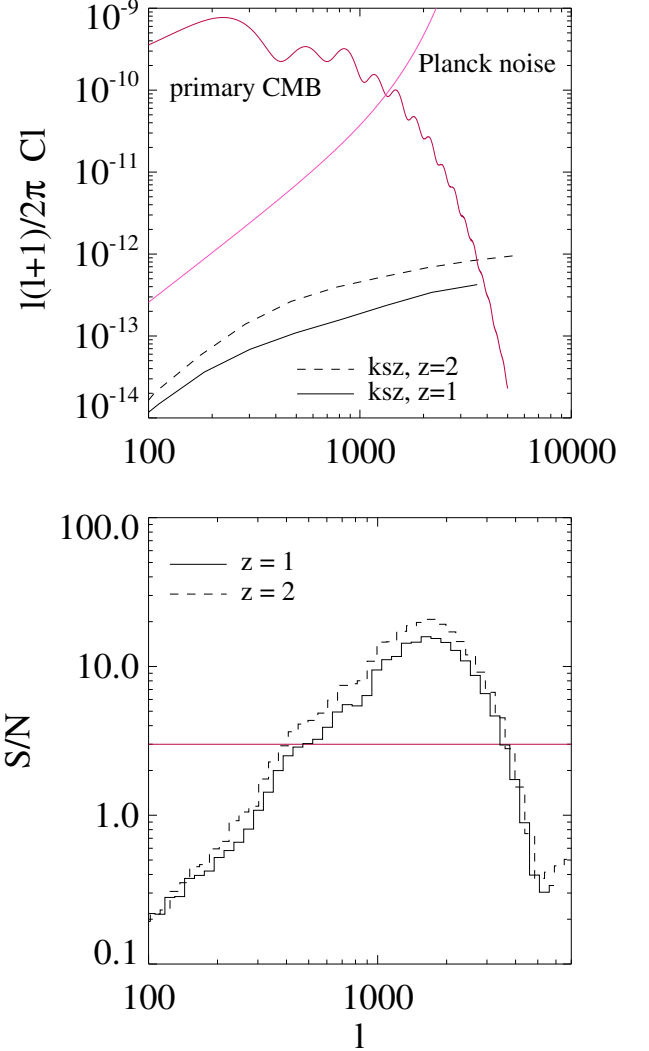


FIG. 4: (Top) Relative strength of kSZ signal, within a box of $\Delta\chi = 1200 \text{ Mpc}/h$. (Bottom) predicted S/N, assuming Planck noise, $\Delta\ell/\ell = 0.1$, $f_{\text{sky}} = 0.8$.

is Sensitivity per beam solid angle, $\theta_{\text{FWHM}} \sim 5'$ is the effective beam FWHM, $W_l = \exp[-\ell(\ell + 1)/2\ell_{\text{beam}}^2]$ is the smoothing window function, with $\ell_{\text{beam}} = \sqrt{8 \ln 2}/\theta_{\text{FWHM}}$. We choose $f_{\text{sky}} = 0.8$, since it is feasible for 21 cm intensity mapping to survey large sky areas. We choose $\Delta\ell/\ell = 0.1$. And for $C_l^{\text{kSZ}, \Delta z}$, we choose two bins of size 1200 Mpc/h, centered at redshift 1,2 respectively.

In Fig.4, we plot the S/N level for the two redshift bins. The S/N will exceeds 3 from $\ell \sim 500 - 3000$. The overall S/N for $z = 1$ is 45, and for $z = 2$ is 59.

Since we only use the correlation calculated from tidal reconstructed field, the S/N shall be higher for $z = 2$ combining tidal reconstructed field and foreground filtered field.

VII. CONCLUSION

In this paper, we discuss the possibility of cross correlating kSZ signal with 21 cm intensity mapping as a new probe to study baryon distributions. A tomographic way of calculating cross correlation with estimated velocity field is applied. Correlation results are presented for redshift 1 and 2, considering foreground noises, finite telescope resolution, and redshift space distortions. The latter two will not matter much. However, the foreground noise will smear the correlation on large scales while leaving sufficient correlation on smaller scales such as $\ell \sim 1000$. In order to study the large scale baryon distribution, we recover modes lost in foregrounds with a 3D tidal reconstruction and obtain a $r > 0.6$ correlation for $\ell \sim 100 - 2000$. After the reconstruction, we will likely be able to distinguish cross correlation signals from $\ell \gtrsim 500$. Assuming Planch noise, the total S/N can reach 45 for $z = 1$ and

59 for $z = 2$. This shows a promising future for this method.

VIII. ACKNOWLEDGE

We acknowledge discussions with Kendrick Smith, Matthew Johnson, Wenkai Hu, Tianxiang Mao and Jiawei Shao. The simulations were performed on the BGQ supercomputer at the SciNet HPC Consortium. SciNet is funded by: the Canada Foundation for Innovation under the auspices of Compute Canada; the Government of Ontario; the Ontario Research Fund – Research Excellence; and the University of Toronto. Research at the Perimeter Institute is supported by the Government of Canada through Industry Canada and by the Province of Ontario through the Ministry of Research & Innovation. The Dunlap Institute is funded through an endowment established by the David Dunlap family and the University of Toronto.

-
- [1] R. J. Cooke, M. Pettini, R. A. Jorgenson, M. T. Murphy, and C. C. Steidel, *ApJ* **781**, 31 (2014), 1308.3240.
 - [2] G. Hinshaw, D. Larson, E. Komatsu, D. N. Spergel, C. L. Bennett, J. Dunkley, M. R. Nolta, M. Halpern, R. S. Hill, N. Odegard, et al., *ApJS* **208**, 19 (2013), 1212.5226.
 - [3] E. Komatsu, K. M. Smith, J. Dunkley, C. L. Bennett, B. Gold, G. Hinshaw, N. Jarosik, D. Larson, M. R. Nolta, L. Page, et al., *ApJS* **192**, 18 (2011), 1001.4538.
 - [4] G. Hinshaw, D. Larson, E. Komatsu, D. N. Spergel, C. L. Bennett, J. Dunkley, M. R. Nolta, M. Halpern, R. S. Hill, N. Odegard, et al., *ApJS* **208**, 19 (2013), 1212.5226.
 - [5] U.-L. Pen, *ApJ* **510**, L1 (1999), astro-ph/9811045.
 - [6] A. M. Soltan, *A&A* **460**, 59 (2006), astro-ph/0604465.
 - [7] J. N. Bregman, *ARA&A* **45**, 221 (2007), 0706.1787.
 - [8] J. K. Werk, J. X. Prochaska, J. Tumlinson, M. S. Peeples, T. M. Tripp, A. J. Fox, N. Lehner, C. Thom, J. M. O’Meara, A. B. Ford, et al., *ApJ* **792**, 8 (2014), 1403.0947.
 - [9] R. A. Sunyaev and Y. B. Zeldovich, *Comments on Astrophysics and Space Physics* **4**, 173 (1972).
 - [10] R. A. Sunyaev and I. B. Zeldovich, *MNRAS* **190**, 413 (1980).
 - [11] E. T. Vishniac, *ApJ* **322**, 597 (1987).
 - [12] M. Fukugita and P. J. E. Peebles, *ApJ* **616**, 643 (2004), astro-ph/0406095.
 - [13] J. C. Hill, S. Ferraro, N. Battaglia, J. Liu, and D. N. Spergel, *ArXiv e-prints* (2016), 1603.01608.
 - [14] S. Ferraro, J. C. Hill, N. Battaglia, J. Liu, and D. N. Spergel, *ArXiv e-prints* (2016), 1605.02722.
 - [15] K. Bandura, G. E. Addison, M. Amiri, J. R. Bond, D. Campbell-Wilson, L. Connor, J.-F. Cliche, G. Davis, M. Deng, N. Denman, et al., in *Society of Photo-Optical Instrumentation Engineers (SPIE) Conference Series* (2014), vol. 9145 of *Society of Photo-Optical Instrumentation Engineers (SPIE) Conference Series*, p. 22, 1406.2288.
 - [16] Y. Xu, X. Wang, and X. Chen, *ApJ* **798**, 40 (2015), 1410.7794.
 - [17] <http://www.acru.ukzn.ac.za/hirax/>.
 - [18] T. Di Matteo, B. Ciardi, and F. Miniati, *MNRAS* **355**, 1053 (2004), astro-ph/0402322.
 - [19] K. W. Masui, E. R. Switzer, N. Banavar, K. Bandura, C. Blake, L.-M. Calin, T.-C. Chang, X. Chen, Y.-C. Li, Y.-W. Liao, et al., *ApJ* **763**, L20 (2013), 1208.0331.
 - [20] E. R. Switzer, T.-C. Chang, K. W. Masui, U.-L. Pen, and T. C. Voytek, *ApJ* **815**, 51 (2015), 1504.07527.
 - [21] U.-L. Pen, R. Sheth, J. Harnois-Déraps, X. Chen, and Z. Li, *ArXiv e-prints* (2012), 1202.5804.
 - [22] H.-M. Zhu, U.-L. Pen, Y. Yu, X. Er, and X. Chen, *ArXiv e-prints* (2015), 1511.04680.
 - [23] J. Shao, P. Zhang, W. Lin, Y. Jing, and J. Pan, *MNRAS* **413**, 628 (2011), 1004.1301.
 - [24] J. Harnois-Déraps, U.-L. Pen, I. T. Iliev, H. Merz, J. D. Emberson, and V. Desjacques, *MNRAS* **436**, 540 (2013), 1208.5098.
 - [25] L. B. Newburgh, G. E. Addison, M. Amiri, K. Bandura, J. R. Bond, L. Connor, J.-F. Cliche, G. Davis, M. Deng, N. Denman, et al., in *Society of Photo-Optical Instrumentation Engineers (SPIE) Conference Series* (2014), vol. 9145 of *Society of Photo-Optical Instrumentation Engineers (SPIE) Conference Series*, p. 91454V, 1406.2267.
 - [26] X. Chen, *International Journal of Modern Physics Conference Series* **12**, 256 (2012), 1212.6278.
 - [27] A. Lewis, A. Challinor, and A. Lasenby, *Astrophys. J.* **538**, 473 (2000), astro-ph/9911177.
 - [28] Planck Collaboration, R. Adam, P. A. R. Ade, N. Aghanim, M. Arnaud, M. Ashdown, J. Aumont, C. Baccigalupi, A. J. Banday, R. B. Barreiro, et al., *ArXiv e-prints* (2015), 1502.01587.